Journal of the European Ceramic Society 21 (2001) 211–218

www.elsevier.com/locate/jeurceramsoc

Indentation crack profiles in silicon nitride

Tanja Lube

Institut für Struktur- und Funktionskeramik, Montanuniversität Leoben, Peter-Tunner-Strasse 5, A-8700 Leoben, Austria

Received 19 May 2000; received in revised form 28 June 2000; accepted 8 July 2000

Abstract

Indentation crack profiles that form under Vickers and Knoop indentations in silicon nitride were investigated. Two different experimental techniques were used to obtain a complete representation of the radial/median as well as the lateral crack system and the plastic deformation zone as a function of indentation load. Vickers indentation cracks exhibit a load dependent shape. At low loads two seperate radial cracks form per median plane, at high loads these cracks merge beneath the hardness impression to form an annular crack. Lateral cracks appear much closer to the surface than frequently assumed. Knoop cracks are nearly semielliptical. The crack aspect ratio and the aspect ratio of the elongated wedge-shaped plastic deformation zone are load dependent.

Keywords: Fracture; Indentation; Optical microscopy; Si_3N_4; Toughness

Indentation Crack Profiles in Silicon Nitride

Tanja Lube
Institut für Struktur- und Funktionskeramik, Montanuniversität Leoben, Peter-Tunner-Strasse 5, A-8700 Leoben, Österreich

Abstract
Indentation crack profiles that form under Vickers- and Knoop indentations in silicon nitride were investigated. Two different experimental techniques were used to obtain a complete representation of the radial/median as well as the lateral crack system and the plastic deformation zone as a function of indentation load. Vickers indentation cracks exhibit a load dependent shape. At low loads two separate radial cracks form per median plane, at high loads these cracks merge beneath the hardness impression to form an annular crack. Lateral cracks appear much closer to the surface than frequently assumed. Knoop cracks are nearly semi-elliptical. The crack aspect ratio and the aspect ratio of the elongated wedge-shaped plastic deformation zone are load dependent.

Keywords: Si_3N_4 (D), indentation, fracture (C), toughness (C), optical microscopy (B)

1 Introduction

Cracks associated with Vickers or Knoop hardness impressions are widely used as artificial defects of "known" size for the fracture toughness measurement of ceramics. A voluminous literature1-6 exists on the quantitative relations between the surface crack length of indentation cracks and the fracture toughness. These analyses usually involve different assumptions about crack and deformation zone geometry, some of which may not be applicable for a given material.
Under sharp indenters two distinct types of cracks (Fig. 1) were found to form in planes perpendicular to the indented surface: shallow, surface cracks (also referred to as Palmqvist-cracks[7] or radial cracks[8]) emerging from the corners of the hardness impression and half-penny (or median/radial[8]) cracks. To distinguish between these two crack systems, a formal criterion based on the crack-length / indent diagonal ratio was proposed[3]. These different crack geometries were detected by layer-by-layer removal in hard metals[4, 5] and some ceramics[9-14] or by decoration techniques[14-18]. Most of the experience with indentation cracks results from experiments with glass, which is - with respect to indentation fracture - an inadequate model material for polycrystalline ceramics, as COOK & PHARR[8] pointed out.
Only few papers deal with systematic investigations of the crack shape as a function of indentation load. The results for polycrystalline transforming ceramics[8, 14] suggest that radial (or kidney-) cracks form at low indentation loads and finally merge to half-penny geometry above a characteristic threshold load. There is some evidence that this behaviour is general also for the elastic/plastic contact fracture in non-transforming ceramics[13].

It is the goal of the present work to investigate the influence of the indentation load on the geometry of indentation crack profiles under Vickers and Knoop indentations in silicon nitride systematically. Two different experimental techniques are used to create a complete representation of crack profiles, lateral cracks and the plastic zone.

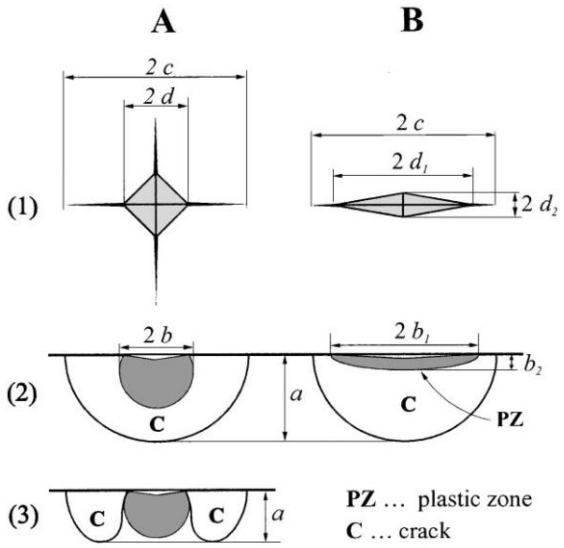

Fig. 1. Schematic of (A) Vickers and (B) Knoop indentation cracks. (1) shows the appearance of the indented surface, (2) gives a cross-sectional view of median/radial cracks and (3) depicts Palmqvist cracks.

2 Investigated material and experimental procedures

The experiments were performed on a commercial gas pressure sintered silicon nitride doped with approx. 3 weight% MgO provided by ESK, Kempten, BRD. Young's modulus $E = 306{,}5 \pm 0{,}3$ GPa was determined by a resonant beam technique[21], fracture toughness $K_c = 6{,}4 \pm 0{,}6$ MPa$\sqrt{m}$ was measured using the SEVN-B method[22].

For some indentation experiments standard flexural specimens were machined from larger billets according to DIN 51 110[23].

All indentations were made into mirror polished surfaces. A Zwick hardness tester 3212 was used up to a load of 294 N. During these experiments the maximum load was reached after 5 s, the dwelling time was 10 s. Indentations with higher loads were made with a miniature universal testing machine ET500 (Engineering Systems, UK) under the same conditions. Vickers cracks produced with loads between 29 N and 981 N were investigated. The loads for Knoop cracks ranged from 29 N to 294 N.

Where required, indented bars were broken in flexural mode on a Zwick Z010/TN2A testing machine on supports with 40 mm lower and 20 mm upper span. A crosshead speed of 0,1 mm/min was used.

Two different experimental techniques were used to investigate the crack patterns produced by Vickers- or Knoop indenters: a decoration process and a serial sectioning technique.

2.1 Decoration of cracks

The decoration of the indentation cracks was performed following the method proposed by JONES ET AL.[17], who also give a detailed description of the method. The indentations were made into a drop of saturated lead acetate solution placed on the centre of the mirror polished tensile surface of a flexural specimens. Care was taken to align one indentation diagonal par-

allel to the specimen's long edge. After removal of the indenter the excess lead acetate solution was allowed to dry on the specimens surface. Drying was completed at 105°C for 15 min in a oven. The specimens were then broken in 4-point-flexure mode with the original indentation crack acting as failure origin.

The portions of the indentation crack that are opened during the indentation cycle or after removal of the indenter are impregnated by the lead acetate solution. On the back-scattered electron image of a SEM these regions appear lighter than the surrounding ceramic fracture surface.

The lead acetate solution penetrates the crack by capillary action and/or diffusion. A good quality decoration depends on the time available for this processes. It has to be ensured that the solution is dry at the moment of fracture to avoid further spreading on the fracture surface. It can be expected that the crack extension is slightly underestimated by the measurement of decoration profiles.

2.2 Serial Sectioning

Investigations of crack profiles by serial sectioning were reported by several authors[9-14]. The contour of the indentation crack is revealed by removing layers of material by ceramographic polishing. The common method is to start from the surface into which the indentations was made, see Fig. 2 (A). Here a different strategy was applied: the layer-by-layer removal was started in a plane perpendicular to the indented surface and to one of the indentation cracks, as depicted in Fig. 2 (B). Some of the difficulties associated with the "classic" method (polishing from the top) are thus avoided:

- The amount of material removed (t_z) can be accurately determined from the remaining crack pattern ($c^*(t_z)$), whereas the exact measurement of t_x is difficult.
- Since the measured quantity $2c(t_x)$ decreases with increasing depth t_x, the deepest point of the crack profile, i.e. the crack depth a, is likely to be missed with the classic method.
- Information about the location and the extension of lateral cracks are readily gained by transverse sectioning while they may cause chipping during polishing from the top.

An automatic ceramographic polishing equipment (by Struers) was used for the layer-by-layer removal. For each layer four polishing steps with diamond suspension from 15µm to 1 µm were performed.

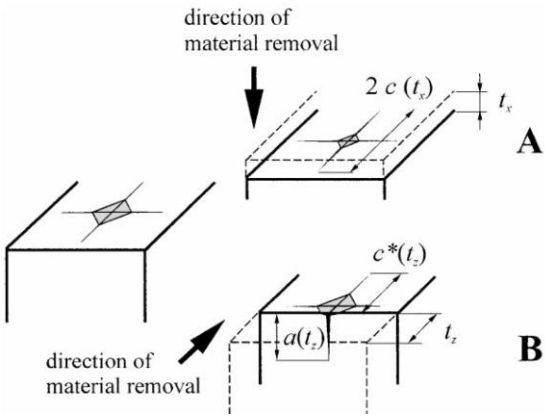

Fig. 2. Serial sectioning of indentation cracks. (A) conventional method, (B) method used in this work.

During the polishing the residual stresses that keep the indentation cracks open may relax leading to closure of the cracks. But at the same time the edge rounding effect usually observed during ceramographic preparation enlarges the cracks. The polishing parameters (mainly the force acting on the polished sections) have to be chosen in such a way that break-out of grains at the crack tip is minimised. Since the investigated material is fine-grained effects of break-out are believed to be smaller than the measuring error.

3 Results

3.1 Vickers indenter

Typical values for the characteristics of Vickers indents and indentation cracks are compiled in Fig. 3. The surface crack lengths *c* measured on the decorated crack profiles turned out to be slightly longer than those measured on polished surfaces. This indicates that a nearly complete impregnation of the cracks was achieved during the decoration procedure. Crack depths *a* measured on decorated crack profiles and determined by serial sectioning do correspond within the experimental scatter. Note that the ratio crack depth / crack length, $e = a/c$, decreases with increasing indentation load.

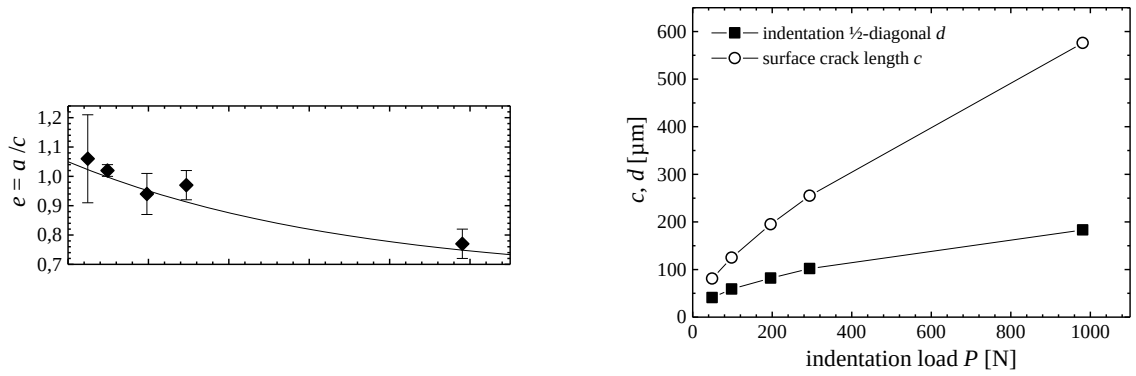

Fig. 3. Characteristics of Vickers indentations and indentation cracks. *d* indentation half-diagonal, *c* surface crack length, *a* crack depth. Each data point represents the mean of at least ten measurement for *c* and *d* and three measurement for *a* respectively.

Profiles of different Vickers-cracks as revealed by decoration with lead acetate can be seen in Fig. 4. Micrographs taken during the serial sectioning of a crack made with 196 N (HV20) are shown in Fig. 5. For cracks introduced with loads of 98 N or higher, the results of the serial sectioning experiments can be summarized in an schematic top- and section-view as depicted in Fig. 6.

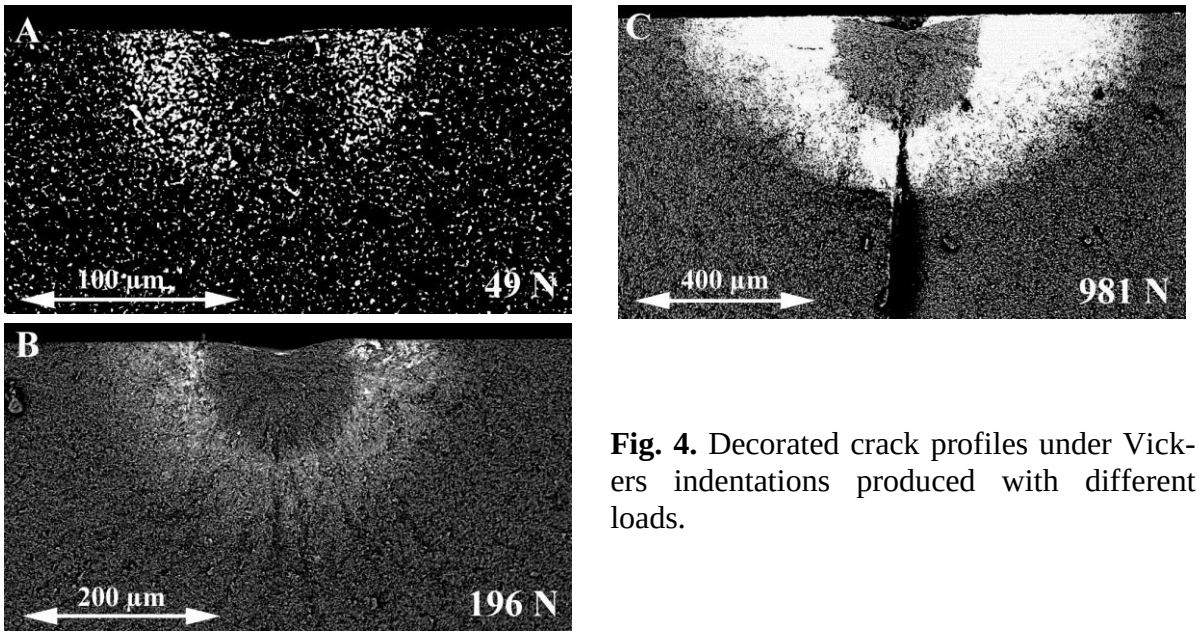

Fig. 4. Decorated crack profiles under Vickers indentations produced with different loads.

The decoration of a 49 N-crack, Fig. 4 (A), suggests that the two crack segments (radial cracks according to the definition given by COOK & PHARR[8], or kidney cracks[14]) emerging from the corners of the indentation do not meet below the indentation centre. This may be the result of an incomplete decoration. The serial sectioning proved that in some cases only crack segments are present, while annular cracks – like for the high-load indentations – or irregularities like two inclined cracks occur in other cases. Separate radials were found for all 29 N-indentations.

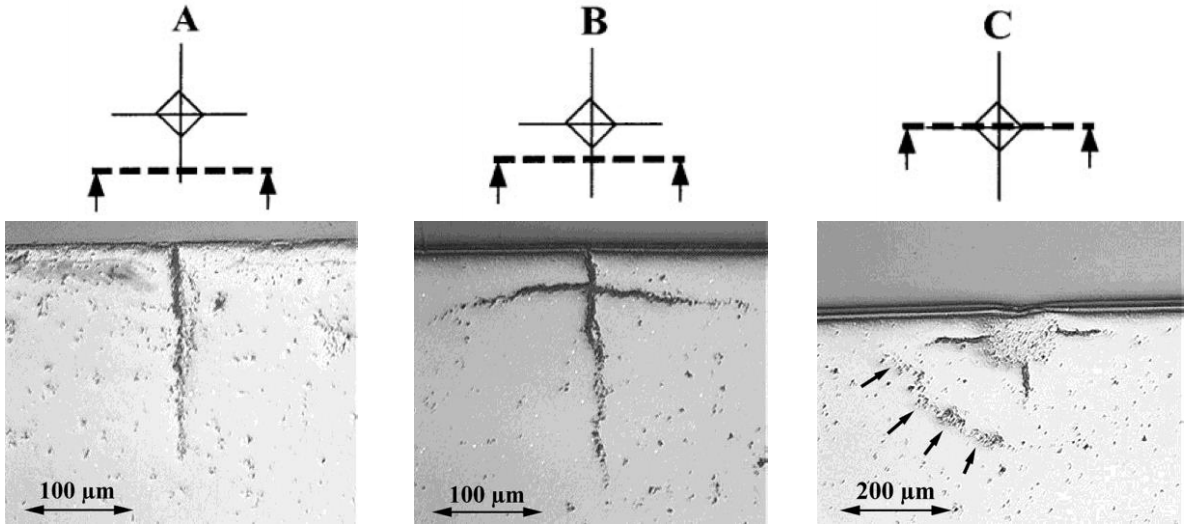

Fig. 5. Different stages of the serial sectioning of a Vickers indentation crack made with 196 N. The position of the section in relation to the indent is shown in the samll sketches above the micrograph. In (C), the trace of the second, perpendicular crack is indicated by arrows.

A core zone with the shape of a spherical segment immediately below the indentation is not decorated by lead acetate and appears dark in Fig. 4. In this zone compressive stresses prevail

during the indentation cycle. Cracks cannot grow into this core zone. On the polished sections, Fig. 5 (C) the plastic zone can be detected by the enhanced break-out on polishing. This may be due to severe damage caused by the high compressive stresses. SEM investigations revealed micro-cracks at grain facets within this region. The compressive stresses are not - or only partially - relieved during the polishing steps. Small secondary indentations (e.g. made with 19 N into the core zone of a 981 N crack) placed into the core zone do not produce cracks, whereas they show cracks when introduced into normal polished surfaces.
Shallow lateral cracks were only found for indentation loads higher than 29 N. They extend nearly to the tips of the annular or radial cracks, Fig. 5 (C) and Fig. 6.

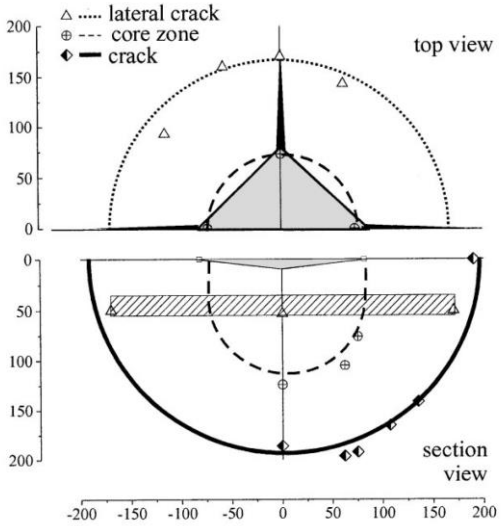

Fig. 6. Schematic top- and cross-sectional view of the 196 N Vickers indentation crack system. Diamonds and the through line indicate the front of the annular crack, the dashed line marks the core zone. The circular front of the lateral crack is indicated by a dotted line and triangles on the top view, the region were they occur below the surface is hatched in the section view.

3.2 Knoop indenter

For the Knoop-cracks too, the correspondence of crack dimensions measured with different experimental techniques is satisfactory. By inspection of the polished specimen surface it was not possible to detect cracks associated with 29 N and 49 N indentations. Decoration proved that these cracks grow just to a length similar to the long indentation diagonal. Typical values for the characteristics of Knoop indents and indentation cracks can be seen in Fig. 7. For these cracks the ratio $e = a/c$ increases with increasing indentation load.
Profiles of different decorated Knoop-cracks are shown in Fig. 8. In this pictures the indentation itself is so shallow that it can not be made out. The extension of the long indentation diagonals d_1 is therefore marked with dashed lines.
Knoop indentations are much shallower than Vickers indentations produced with the same load. Due to recovery of the elastic deformation after the removal of the indenter, the remaining impression is less deep than the geometric depth (i.e. calculated from the indenter geometry and the measured indentation diagonals) of the impression[24]. The core zone for Knoop indentations has the shape of an elongated wedge. It extends over nearly the same length as the long indentation diagonal in its dimension parallel to the surface. The depth of the zone is approx. four times the geometric depth of the hardness impression.

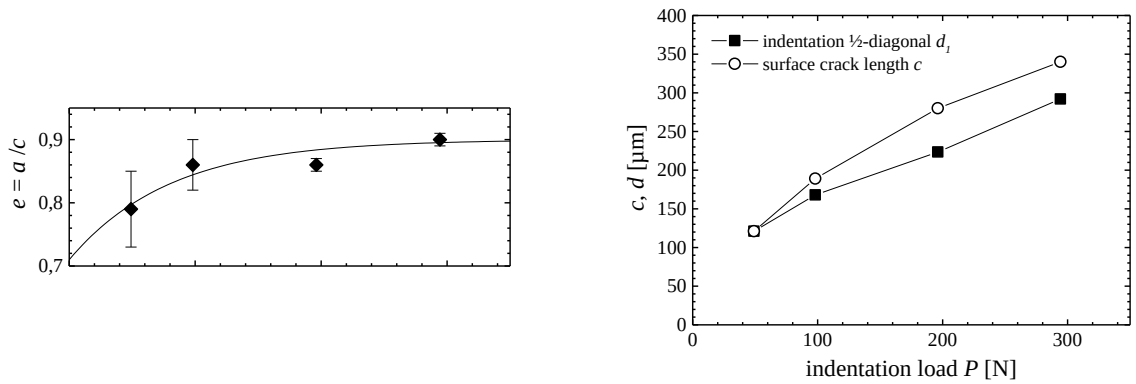

Fig. 7. Characteristics of Knoop indentations and indentation cracks. d_1 indentation half-diagonal, *c* surface crack length, *a* crack depth. Each data point represents the mean of at least ten measurement for *c* and *d* and three measurement for *a* respectively.

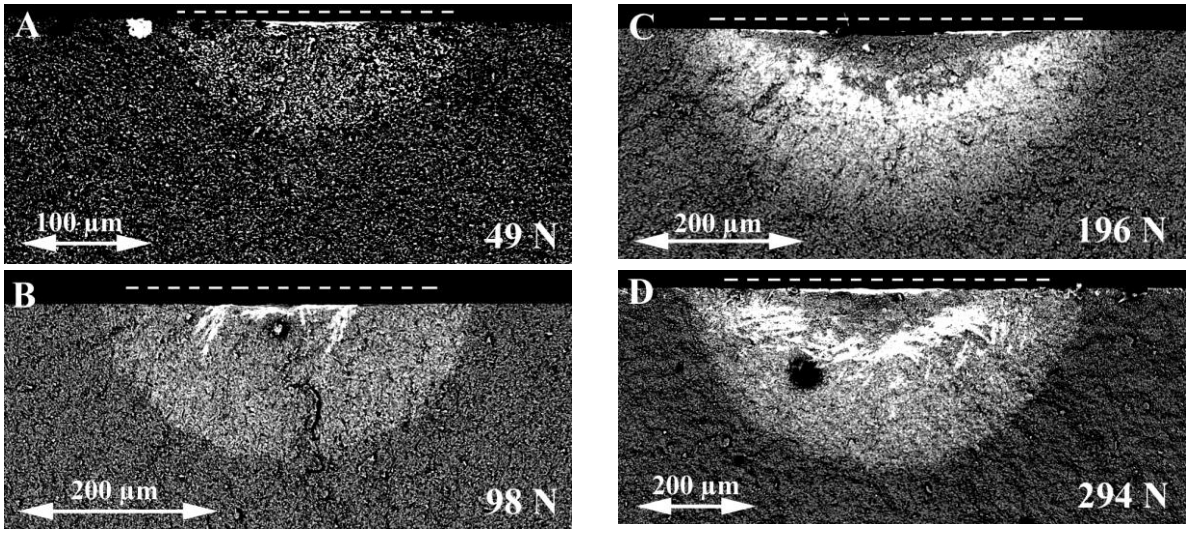

Fig. 8. Decorated crack profiles under Knoop indentations produced with different loads. The dashed lines indicate the extension of the long indentation diagonal.

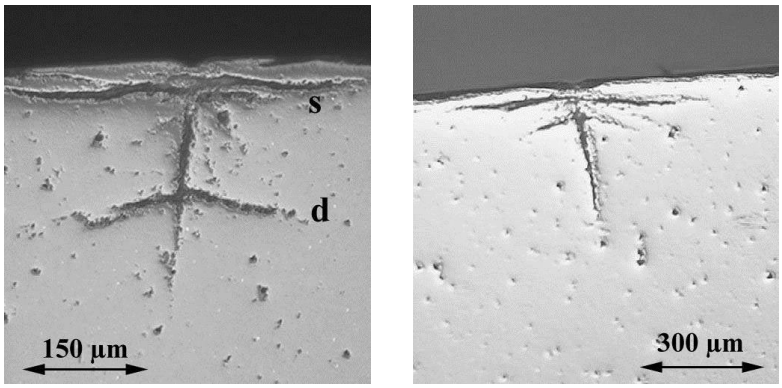

Fig. 9. Multiple lateral cracks under a 294 N Knoop indentation: **s** shallow laterals, **d** deep laterals.

Below the plastic zone a very light region can be observed in Fig. 8 (C) & (D). Serial sectioning revealed that the lateral cracks intersect with the half-elliptical crack in this zone. For Knoop-indentations multiple lateral cracks, like those shown in Fig. 9, are typical. Especially at indentation loads higher than 98 N shallow lateral cracks are often accompanied by deep laterals.

4 Discussion

4.1 Vickers cracks

Indentation cracks are commonly described[25] as half-penny cracks wedged open by a point load P acting at the centre of a half-penny surface crack with radius c. This model leads to

$$K_c = \chi \cdot \frac{P}{c^{3/2}} \qquad (1)$$

for the fracture toughness K_c. The residual stress parameter χ depends on the elastic/plastic deformation behaviour of the material and the indenter geometry. If both the fracture toughness K_c and the residual stress parameter χ are constant the quantity $P/c^{3/2}$ is independent of indentation load. In general, deviations from this behaviour can be explained by two effects: the deformation fields are not self similar for different indentations loads and thus lead to crack driving stress fields (characterized by the quantity χ) that vary with indentation load, or the material exhibits a R-curve, i.e. the fracture toughness increases with crack extension.
Fig. 10 shows that within the experimental scatter $P/c^{3/2}$ for Vickers cracks is constant over the range of investigated indentation loads (49 N … 984 N). The point force model seems to be an appropriate description of Vickers cracks in the investigated silicon nitride, even though a change in crack geometry was observed.

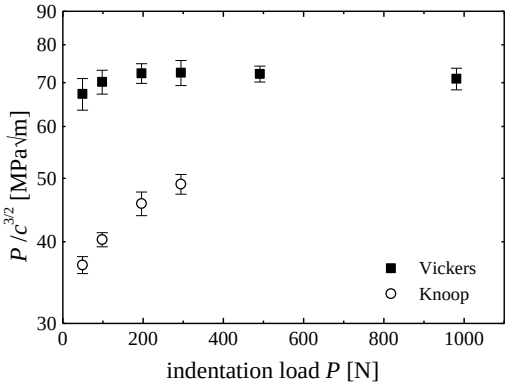

Fig. 10. Load crack length data for Vickers- and Knoop indentation cracks plotted according to eq. (1).

Radial (or Palmqvist) indentation cracks in ceramics have been reported by different authors. Jones et al.[17], Pajares et al.[26] or Cook et al.[12] observed them in different zirconia ceramics, Shetty et al.[9] in glass ceramic and Lankford[10] in alumina. The transition from two separate radials per median plane to one single annular crack like in the investigated silicon nitride has been observed in Ce-TZP by Matsumoto[11], in 4Y-PSZ by Pajares et al.[26] and in a HPSN by El Aslabi et al.[13]. These observation suggest that the general cracking sequence during the indentation process for such polycrystalline ceramics is governed by primary radial crack formation

and eventual impingement of these cracks below the impression centre once a critical load is surpassed. Ledges just below the indentation centre like in Fig. 4 (C) are often observed and confirm this sequence.

The existence of radial cracks that form independently from median cracks can be concluded from the analysis of the indentation stress field by CHIANG, MARSHALL & EVANS[27] (CME). From their analysis it follows that the driving forces for radial crack formation are greater than for median crack formation. COOK & PHARR[8] observed that these cracks may grow during the loading cycle as well as during the unloading cycle in single crystals with a sufficiently high ratio of Young's modulus/hardness, E/H. They do not report if a transition to annular cracks did occur in the materials they investigated.

An explanation for the observed cracking behaviour with the transition from radial to annular cracks is provided by PAJARES ET AL.[26] for the special case of a transformation-toughened 4Y-PSZ. During the indentation cycle the stress-induced monoclinic to tetragonal phase transformation leads to a volume increase around the indentation. As a result a hydrostatic stress field builds up originating in the plastic deformation zone underneath the hardness impression with its centre at a certain depth below the surface. Such a behaviour violates some of the assumptions of the standard indentation theory[25, 27], i.e. that plastic deformation processes are volume-conserving and that residual stresses arise only due to elastic accommodation of the indent volume. The additional radial decreasing hydrostatic stress field modifies the generally assumed point force model residual stress field. Consequently the crack shape is affected by this combined stress field.

According to this model the transition from the radial crack geometry to the annular crack geometry occurs if the ratio crack length / indentation diagonal, $c/d = m$ surpasses a minimum value[26]. The quantity m is a measure for the range in which the hydrostatic stress field is effective. The minimum for m is reached at the critical load P^* which varies with toughness K_c and hardness H of the material:

$$P^* = \frac{8m^6}{\chi^4} \cdot \frac{K_c^4}{H^3} \quad . \quad (2)$$

The geometric resemblance of the crack profiles found in the investigated silicon nitride with those reported by PAJARES ET AL.[26] suggests an application of their model to silicon nitride. With H = 14, 6 GPa, K_{Ic} = 6,4 MPa, $P^* \approx 100$ N and $\chi = \delta \cdot (E/H)^{1/2}$ with $\delta = 0{,}016^2$, eq. (2) gives $m \approx 1$. This corresponds to the m-value reported earlier for non-transforming ceramics[26], but differs significantly from the experimental ratio $m = c/d$ for cracks introduced with loads close to P^*: $c/d\,|_{49N} = 1{,}8$ and $c/d\,|_{98N} = 2{,}2$. Obviously the application of the presented model for the formation of kidney-cracks is not quite appropriate for non-transforming ceramics. This is also supported by the fact, that for $m \approx 1$ the additional hydrostatic stress field is nearly completely confined to the crack-free portion of the plastic deformation zone and should therefore not strongly influence the indentation cracks.

From the size of the un-cracked, compressed core zone it is possible to estimate the radius b of the plastic deformation zone. From the CME analysis[27] of indentation stresses we learn that maximum tensile stresses occur at the border of the plastic zone (relative size $\beta = b/d^*$, where d^* is the radius of a sphere with the volume of the Vickers indentation[24]: $d^* = d \cdot \cot^{0,33}68°/1{,}644$) and that compressive stresses prevail within a smaller core zone. The extension of this zone at the specimens surface (r_c^S) is smaller than its extension beneath

the indentation (r_c^M). As a consequence, the core zone will not be a hemisphere but resemble more an ellipsoid or a spherical segment with its centre offset below the specimens surface. The micrographs in Fig. 4 confirm this. For the theoretical value $\beta \approx 2{,}8$ for silicon nitride[24] the core zone extensions r_c^S and r_c^M are approximately between 78% and 85% of the plastic zone radius b. A first estimation of β from measured geometries of the core zones averaged over all investigated indentation loads (see table 1) yields $\beta \approx 2{,}6$.
Lateral cracks appear at a distance of less than $\beta/2$ below the surface. This behaviour is in excellent agreement with the theoretical predictions for the location of maximum tensile stresses normal to the specimens surface[27] as well as with experimental observations on transparent single crystals[8].

Table 1: Characteristics of the plastic zone of Vickers indentation cracks.

	49 N	98 N	196 N	294 N	981 N
d [µm]	41	58	82	102	183
r_c [µm]	36	58	75	89	176
β	2,5	2,8	2,6	2,4	2,7

It should be mentioned here that the pictures of lateral cracks emerging close to the bottom of the plastic zone as often reported in textbooks[24, 25, 28] represent the experimental observations on soda-lime glass[28, 29] rather than the situation in polycrystalline ceramics. The same may be stated for the cracking sequence. As COOK & PHARR[8] showed the cracking sequence depends on the ratio of Young's modulus / hardness, E/H, of the indented material. The sequence where median cracks precede median/radial- or half-penny-cracks and laterals form upon unloading is typical for glass with a low E/H-ratio. For ceramics with a high E/H-ratio a different sequence with independent radials and lateral cracks forming during the loading cycle may as well take place.

4.2 Knoop cracks

For Knoop-cracks, a strong dependence of $P/c^{3/2}$ on indentation load can be observed in Fig. 10. The simple point force model is not suitable for the fracture mechanical description of such cracks. KEER ET AL.[30] showed that this behaviour can be explained by assuming that Knoop-indentation cracks are opened by a residual pressure that is constant over a semi-elliptical portion of the crack (at the location of the plastic zone) with a load dependent aspect ratio. They calculated plastic zone sizes for different loads so that experimental $P/c^{3/2}$-data for silicon nitride were matched. A comparison of characteristics of plastic zones measured on decorated cracks with these calculated values is plotted in Fig. 11. The load dependence of the length of the plastic zones (b_1/c) cannot be verified due to the lack of data, but the aspect ratio b_1/b_2 follows the trend given by the calculations.

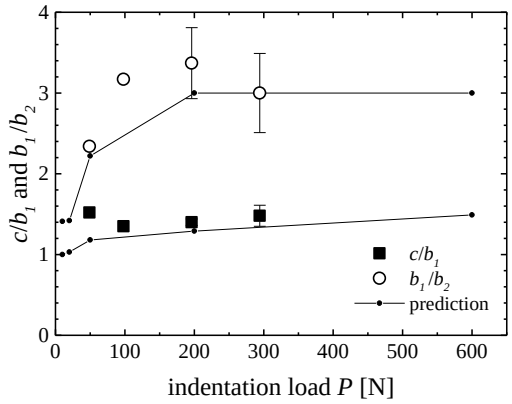

Fig. 11. Comparison of calculated and measured characteristics of the plastic deformation zone of Knoop indentations.

Knoop-cracks are used as artificial flaws of known size in the surface-crack-in-flexure (SCF)[31] technique for measuring fracture toughness. For this testing procedure it is prescribed to remove the contact zone of the indentation by grinding away a surface layer of a thickness of approx. 4,5 … 5 times the indentation depth ($\approx d_1/6$). The decoration experiments confirm that this is indeed enough to remove the plastic zone. The serial sectioning indicates that the shallow lateral cracks located immediately below the plastic zone are then removed too but the deep lateral cracks will however remain.

5 Summary

The geometry of Vickers- and Knoop indentations cracks as a function of indentation load was investigated using two different techniques. Together these techniques produce a complete 3D-respresentation of the indentation crack system.

For Vickers cracks a transition from deep radial cracks emerging from the corners of the indentation to annular cracks surrounding the deformation zone with increasing indentation load was observed. This behaviour is in agreement with in situ observations of cracking sequences in transparent crystals and predictions basing on calculated indentation stress fields. The size of the plastic zone was estimated and found to match the theoretical prediction. Lateral cracks form close to the surface at a depth were tensile stresses normal to the free specimen reach a maximum.

Knoop indentations produce semi-elliptical cracks with load dependent aspect ratio. For these cracks the plastic zone has a load dependent shape and size. Lateral cracks form at low indentation loads, at high loads a deep secondary lateral system is present. The polishing procedure prescribed[31] to remove the plastic zone of Knoop indents will remove the shallow laterals but not the deep lateral cracks.

Acknowledgements
This work was supported by the Bundesministerium für Wissenschaft, Forschung und Verkehr der Republik Österreich under contract no. GZ 49.929/3-II/4/94, "Mechanische Eigenschaften von keramischen Hochleistungswerkstoffen".

References

1. Evans, A.G., Charles, E.A., Fracture Toughness Determination by Indentation. *J. Am. Ceram. Soc.*, 1976, **59**, 371-372
2. Anstis, G.R., Chantiklul, P., Lawn, B.R., Marshall, D.B., A Critical Evaluation of Indentation Techniques for Measuring Fracture Toughness: I, Direct Crack Measurements. *J. Am. Ceram. Soc.*, 1981, **64**, 533-538
3. Niihara, K., Morena, R., Hasselman, D.P.H., Evaluation of K_{Ic} of Brittle Solids by the Indentation Method with Low Crack-to-Indent Ratios. *J. Mat. Sci. Let.*, 1982, **1**, 13-16
4. Laugier, M.T., Palmquist Indentation Crack Analyses for Toughness Determination in WC-Co Composites. *Key Eng. Mat.*, 1989, **32**, 77-84
5. Shetty, D.K., Wright, I.G., Mincer, P.N., Clauer, A.H., Indentation Fracture of WC-Co Cermets. *J. Mat. Sci.*, 1985, **20**, 1873-1882
6. Li, Z., Ghosh, A., Kobayashi, A.S., Bradt, R.C, Indentation Fracture Toughness of Sintered Silicon Carbide in the Palmqvist Crack Regime. *J. Am. Ceram. Soc.*, 1989, **72**, 904-911
7. Palmqvist, S., Rißbildungsarbeit bei Vickers-Eindrücken als Maß für die Zähigkeit von Hartmetallen. *Arch. Eisenhütt.*, 1962, **33**, 629-634
8. Cook, R.F., Pharr, G.M., Direct Observation and Analysis of Indentation Cracking in Glasses and Ceramics. *J. Am. Ceram. Soc.*, 1990, **73**, 787-817
9. Shetty, D.K., Rosenfield, A.R., Duckworth, W.H., Indenter Flaw Geometry and Fracture Toughness Estimates for a Glass-Ceramic. *J. Am. Ceram. Soc.*, 1985, **68**, C282-C284
10. Lankford, J., Threshold Microfracture During Elastic-Plastic Indentation of Ceramics. *J. Mat. Sci.*, 1981, **16**, 1177-1182
11. Matsumo, R.L.K., Evaluation of Fracture Toughness Determination Methods as Applied to Ceria-Stabilized Tetragonal Zriconia Polycrystals. *J. Am. Ceram. Soc.*, 1987, **70**, C366-C368
12. Cook, R.F., Braun L.M., Cannon, W.R., Trapped Cracks at Indentations, Part I: Experiments on Yttria-Tetragonal Zirconia Polycrystals. *J. Mat. Sci.*, 1994, **29**, 2133-2142
13. El Aslabi, A.M., Kleist, G., Steinbrech, R.W., Nickel, H., Evaluation of Indentation Fracture Toughness of Si_3N_4 Using Crack Profile Measurements. *Fortschrittsberichte der DKG*, 1991, **6**, 133-149
14. Kaliszewski, M.S., Behrens, G., Heuer, A.H. et. al., Indentation Studies on Y_2O_3-stabilized ZrO_2: I, Development of Indentation-Induced Cracks. *J. Am. Ceram. Soc.*, 1994, **77**, 1185-1193
15. Liang, K.M., Orange, G., Fantozzi, G., Evaluation by Indentation of Fracture Toughness of Ceramic Materials. *J. Mat. Sci.*, 1990, **25**, 207-214
16. Sullivan, J.D., Lauzon, P.H., Shape Profiles of Cracks Formed Under a Vickers

Pyramid Indenter. *J. Mat. Sci. Lett.*, 1986, **5**, 247-248

17. Jones, S.L., Norman, C.J., Shahani, R., Crack-Profile Shapes Formed Under a Vickers Indent Pyramid. *J. Mat. Sci. Let.*, 1987, **6**, 721-723
18. Hansen, J.J., Cutler, R.A., Shetty, D.K., Virkar, A.V., Indentation Fracture Response and Damage Resistance of Al_2O_3-ZrO_2 Composites Strengthened by Transformation-Induced Residual Stresses. *J. Am. Ceram. Soc.*, 1988, **71**, C501-C505
19. Liu, S.-Y., Chen, I.-W., Fatigue of Yttria-Stabilized Zirconia II: Crack Propagation, Fatigue Striations and Short-Crack Behaviour. *J. Am. Ceram. Soc.*, 1991, **74**, 1206-1216
20. Sgalvo, V.M., Pancheri, P., Crack Decorating Technique for Fracture-Toughness Measurement in Alumina. *J. Eur. Ceram. Soc.*, 1997, **17**, 1697-1706
21. Lins, W., Kaindl, G., Peterlik, H., Kromp, K., A Novel Resonant Beam Technique to Determine the Elastic Moduli in Dependence on Orientation and Temperature up to 2000 C. *Rev. Sci. Instrum.*, 1999, **70**, 3052-3058
22. Damani, R.J., Schuster, C., Danzer, R., Polished Notch Modification of SENB-S Fracture Toughness Testing. *J. Eur. Ceram. Soc.*, 1997, **17**, 1685-1689
23. DIN 51 110, Prüfung von Keramischen Hochleistungswerkstoffen, Teil 1: 4-Punkt-Biegeversuch bei Raumtemperatur, 1990
24. McColm, I.E., *Ceramic Hardness*, Plenum Press, New York & London, 1990, pp. 145 ff.
25. Lawn, B., *Fracture of Brittle Solids*, Cambridge University Press, Cambridge, 1993, pp. 249 ff.
26. Pajares, A., Guiberteau, F., Cumbrera, F.L., Steinbrech, R.W., Dominguez-Rodriguez, A., Analysis of Kidney-shaped Indentation Cracks in 4Y-PSZ. *Acta mater.*, 1996, **44**, 4387-4394
27. Chiang, S.S., Marshall, D.B., Evans, A.G., The Response of Solids to Elastic/Plastic Indentation: I, Stresses and Residual Stresses. *J. Appl. Phys.*, 1982, **53**, 298-311
28. Green, D.J., *An Introduction to the Mechanical Properties of Ceramics*, Cambridge University Press, Cambridge, 1998, pp.274, 275.
29. Smith, S.M., Scattergood, R.O., Crack-Shape Effects for Indentation Fracture Toughness Measurements, *J. Am. Ceram. Soc.*, 1992, **75**, 305-315
30. Keer, L.M., Farris, T.N., Lee, J.-C., Knoop and Vickers Indentation in Ceramics Analysed as a Three-Dimensional Fracture. *J. Am. Ceram. Soc.*, 1986, **69**, 392-396
31. ASTM PS070, Standard Test Methods for the Determination of Fracture Toughness of Advanced Ceramics at Ambient Temperature, 1998